Control Engineering Practice 81 (2018) 43–54

Contents lists available at ScienceDirect

Control Engineering Practice

journal homepage: www.elsevier.com/locate/conengprac

Nonlinear model predictive torque control of PMSMs for high performance applications

Tobias Englert *, Knut Graichen

Institute of Measurement, Control and Microtechnology, Ulm University, 89081 Ulm, Germany

ARTICLE INFO

Keywords:
Nonlinear MPC
Electric machine control
Permanent magnet synchronous machine
Nonlinear constraints
Augmented Lagrangian method
Gradient method
Embedded optimization

ABSTRACT

This contribution presents a nonlinear model predictive control (MPC) scheme for the torque control of permanent magnet synchronous machines. The control scheme is based on the nonlinear dq-model including current-dependent inductivities and provides a desired torque in an energy-efficient way while accounting for constraints on the DC link current, phase currents, and hexagonal voltage constraints. The MPC algorithm uses an augmented Lagrangian method in combination with a real-time gradient method to allow for a computationally efficient solution. Experimental results for a standard industrial drive show the performance, robustness, and computational efficiency of the MPC with a sampling time of 500 μs.

1. Introduction

Permanent magnet synchronous machines (PMSMs) are increasingly used in industrial and automotive drive systems, as they typically achieve a high torque and power density and therefore are suitable drives for highly dynamical and high precision applications such as traction drives, electric power steering systems, or machine tools.

Recently, various model predictive control (MPC) strategies for PMSMs have been developed in order to improve the control performance compared to conventional control strategies such as field-orientated control (FOC) (Schröder, 2009). These approaches can be divided into two categories depending on the working principle of the power electronics.

The finite control set MPC (FCS-MPC) approaches actuate the switches of the power electronics directly, cf. e.g. Geyer (2011), Lang, Yang, Long, Li, and Xu (2016), Liu and Hameyer (2015), Preindl and Bolognani (2013b), Rodriguez et al. (2013) and Xie, Wang, Wang, Xu, Kennel, Gerling, and Lorenz (2015), which limits the control space to a finite set consisting of eight voltage vectors. The basic idea is to evaluate all possible combinations of the control set elements over the prediction horizon using a cost function. Thereby, the discrete nature of voltage inverters is exploited, which leads to low switching frequencies of the power electronics. On the other hand, the sampling time is directly related to the switching frequency. As a consequence, the sampling time must be very small in order to avoid large torque ripples. Furthermore, the number of possible combinations of the control sets elements and therefore the computation time increases exponentially with larger prediction horizons. Although more efficient computation algorithms have been developed recently (Geyer & Quevedo, 2014), torque ripples and short prediction horizons must in general be accepted in the case of FCS-MPC (Preindl & Bolognani, 2015).

Opposed to FCS-MPC, continuous control set MPC (CCS-MPC) is based on a continuous voltage set that is obtained by a modulation stage between the torque controller and the power electronic, cf. e.g. Chai, Wang, and Rogers (2013), Cimini, Bernardini, Bemporad, and Levijoki (2015) and Preindl, Bolognani, and Danielson (2013). The sampling frequency in CCS-MPC is typically much lower than in FCS-MPC, which also implies a lower level of torque ripples. Moreover, the larger sampling time enables longer prediction horizons and therefore a potentially better overall control performance. However, solving the underlying (nonlinear) optimization problem in real-time is still a computational challenge and one of the main reasons why the field of CCS-MPC is still considered being largely unexplored (Geyer, 2016).

In applications, where torque ripples are not critical, FCS-MPC schemes achieve smaller switching losses compared to CCS schemes (Geyer & Quevedo, 2015; Köhler, Manderla, & Malchow, 2017). However, if torque accuracy is important, FCS schemes have to increase the switching and sampling frequency as stated above, which mitigates this advantage of FCS-MPC over CCS-MPC (Geyer, 2016; Geyer & Quevedo, 2015). Moreover, the high switching frequencies of FCS and the correspondingly short sampling times are computationally hard to realize.

In addition to torque accuracy, high performance applications such as electric steering systems require a fast dynamic response to the

* Corresponding author.
E-mail addresses: tobias.englert@uni-ulm.de (T. Englert), knut.graichen@uni-ulm.de (K. Graichen).

https://doi.org/10.1016/j.conengprac.2018.08.023
Received 15 September 2017; Received in revised form 29 August 2018; Accepted 30 August 2018
0967-0661/© 2018 Elsevier Ltd. All rights reserved.

desired torque over a wide operation range, e.g. from standstill to maximum speed while guaranteeing an optimal exploitation of given system constraints. The consideration of all these aspects within a real-time CCS-MPC scheme is, as mentioned before, a challenging problem. For instance, existing CCS-MPC approaches as those mentioned above do not account for DC link current constraints, which are especially important in automotive applications, or do not consider flux weakening or anisotropic machines (Chai et al., 2013; Cimini et al., 2015). Moreover, the prediction horizon is often chosen small enough compared to the system dynamics, in order to cope with the computational effort (Chai et al., 2013; Cimini et al., 2015; Preindl et al., 2013).

In a previous publication of the authors (Englert, Grüner, & Graichen, 2017), a model predictive torque controller (also referred to as MPTC in the literature) for PMSMs was developed that overcomes some of the problems mentioned above. However, saturation and other parasitic effects have not been considered so far. In this contribution, the previously presented MPC scheme (Englert et al., 2017) is extended in various directions. The abovementioned effects are accounted for by considering current-dependent system parameters such as the inductivities that are identified at a PMSM test bench. In addition, the proposed nonlinear MPC scheme considers DC link current constraints as well as the whole control set, i.e. the exact hexagonal voltage constraint and not an approximation of it, as it is typically done.

In view of the given system constraints and the very small sampling time that is typically in the range of a few hundred microseconds, real-time feasibility on embedded hardware is a challenge on its own. In order to overcome this challenges, the nonlinear MPC approach uses an augmented Lagrangian technique to effectively incorporate the various constraints in combination with a real-time gradient method. Experimental results, including a comparison with a standard field-orientated control, show the robustness, performance, and computational efficiency. In particular, the MPC computation times of less than 100 µs on a standard dSpace real-time platform demonstrate the real-time feasibility of the control scheme.

The paper is outlined as follows. Section 2 states the physical PMSM model and the system constraints. Section 3 presents the MPC formulation and the nonlinear optimization algorithm for solving the MPC problem. The experimental framework including the PMSM test bench, parameter identification, and load estimation is presented in Section 4. Finally, experimental results in Section 5 illustrate the MPC's performance in comparison to a standard field-oriented controller. The paper concludes with a short summary and an outlook to further work.

2. Problem statement

This section derives the electrical and mechanical subsystems of the PMSM model and illustrates the parameter dependencies. In addition, the constraints that the MPC has to account for are presented.

2.1. Model design

This paper considers a PMSM that is driven by a two-level voltage source inverter (VSI), as shown in Fig. 1. The VSI is assumed to be ideal in the sense, that it compensates for parasitic effects by itself. The electrical behavior of a PMSM is typically described by the dq-model assuming constant electrical parameters such as inductivities and permanent flux linkage, see e.g. Schröder (2009). However, in general, these parameters are not constant. Therefore, the basic voltage equations

$$u_\mathrm{d} = Ri_\mathrm{d} + \tfrac{\mathrm{d}}{\mathrm{d}t}\psi_\mathrm{d}(i_\mathrm{d}, i_\mathrm{q}) - \omega\psi_\mathrm{q}(i_\mathrm{d}, i_\mathrm{q}) \tag{1a}$$

$$u_\mathrm{q} = Ri_\mathrm{q} + \tfrac{\mathrm{d}}{\mathrm{d}t}\psi_\mathrm{q}(i_\mathrm{d}, i_\mathrm{q}) + \omega\psi_\mathrm{d}(i_\mathrm{d}, i_\mathrm{q}) \tag{1b}$$

with the electrical rotor speed ω, the dq-currents i_d and i_q, the dq-voltages u_d and u_q, the stator resistance R, and the flux linkages

$$\psi_\mathrm{d}(i_\mathrm{d}, i_\mathrm{q}) = \psi_\mathrm{P}(i_\mathrm{q}) + L_\mathrm{d}(i_\mathrm{d}, i_\mathrm{q})i_\mathrm{d} \tag{2a}$$

$$\psi_\mathrm{q}(i_\mathrm{d}, i_\mathrm{q}) = L_\mathrm{q}(i_\mathrm{d}, i_\mathrm{q})i_\mathrm{q} \tag{2b}$$

are considered.

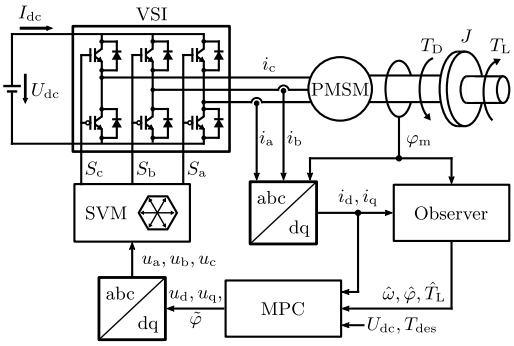

Fig. 1. Schematic representation of the PMSM drive system.

The dq-inductivities L_d and L_q as well as the permanent flux linkage ψ_p in general depend on the dq-currents and in general also on the angle of the rotor, cf. e.g. Ebersberger and Piepenbreier (2012). However, the angular dependency is not considered in this paper, in order to keep both the modeling effort and the computational complexity within reasonable limits. Also note that resistance R depends on the temperature. This effect is neglected as well, as the thermal dynamics of the PMSM is slow compared to its current dynamics.

Evaluating the derivatives in the voltage equations (1) and (2) leads to the differential equations

$$u_\mathrm{d} = Ri_\mathrm{d} + \underbrace{\tfrac{\partial\psi_\mathrm{d}(i_\mathrm{d},i_\mathrm{q})}{\partial i_\mathrm{d}}}_{L_\mathrm{dd}}\tfrac{\mathrm{d}i_\mathrm{d}}{\mathrm{d}t} + \underbrace{\tfrac{\partial\psi_\mathrm{d}(i_\mathrm{d},i_\mathrm{q})}{\partial i_\mathrm{q}}}_{L_\mathrm{dq}}\tfrac{\mathrm{d}i_\mathrm{q}}{\mathrm{d}t} - \omega\psi_\mathrm{q}\left(i_\mathrm{d}, i_\mathrm{q}\right) \tag{3a}$$

$$u_\mathrm{q} = Ri_\mathrm{q} + \underbrace{\tfrac{\partial\psi_\mathrm{q}(i_\mathrm{d},i_\mathrm{q})}{\partial i_\mathrm{d}}}_{L_\mathrm{qd}}\tfrac{\mathrm{d}i_\mathrm{d}}{\mathrm{d}t} + \underbrace{\tfrac{\partial\psi_\mathrm{q}(i_\mathrm{d},i_\mathrm{q})}{\partial i_\mathrm{q}}}_{L_\mathrm{qq}}\tfrac{\mathrm{d}i_\mathrm{q}}{\mathrm{d}t} + \omega\psi_\mathrm{d}\left(i_\mathrm{d}, i_\mathrm{q}\right) \tag{3b}$$

for the dq-currents i_d and i_q. The partial derivatives of the flux linkages with respect to the dq-currents form the differential inductivities L_dd, L_qq, L_dq, and L_qd, respectively. Explicitly solving the system (3) for $\frac{\mathrm{d}i_\mathrm{d}}{\mathrm{d}t}$ and $\frac{\mathrm{d}i_\mathrm{q}}{\mathrm{d}t}$ would require the inversion of the differential inductivity matrix, which renders the resulting ordinary differential equations (ODEs) too complex for a nonlinear MPC approach running in real-time.

Two reasonable assumptions can be made to simplify (3). The differential cross coupling inductivities L_dq and L_qd are typically about one order of magnitude smaller than L_dd and L_qq (Ebersberger & Piepenbreier, 2012; Kellner & Piepenbreier, 2011). Furthermore, L_dd and L_qq correspond closely to the absolute inductivities L_d or L_q. Small differences between these quantities only occur for higher currents, see e.g. Kellner and Piepenbreier (2011). These observations and considering (2) and (3) lead to the approximations

$$L_\mathrm{dd} = \tfrac{\partial\psi_\mathrm{d}(i_\mathrm{d},i_\mathrm{q})}{\partial i_\mathrm{d}} = L_\mathrm{d}\left(i_\mathrm{d}, i_\mathrm{q}\right) + \tfrac{\partial L_\mathrm{d}(i_\mathrm{d},i_\mathrm{q})}{\partial i_\mathrm{d}}i_\mathrm{d} \approx L_\mathrm{d} \tag{4a}$$

$$L_\mathrm{qq} = \tfrac{\partial\psi_\mathrm{q}(i_\mathrm{d},i_\mathrm{q})}{\partial i_\mathrm{q}} = L_\mathrm{q}\left(i_\mathrm{d}, i_\mathrm{q}\right) + \tfrac{\partial L_\mathrm{q}(i_\mathrm{d},i_\mathrm{q})}{\partial i_\mathrm{q}}i_\mathrm{q} \approx L_\mathrm{q} \tag{4b}$$

$$L_\mathrm{dq} = \tfrac{\partial\psi_\mathrm{d}(i_\mathrm{q},i_\mathrm{q})}{\partial i_\mathrm{d}} = \tfrac{\partial\psi_\mathrm{P}(i_\mathrm{q})}{\partial i_\mathrm{q}} + \tfrac{\partial L_\mathrm{d}(i_\mathrm{q},i_\mathrm{q})}{\partial i_\mathrm{q}}i_\mathrm{d} \approx 0 \tag{4c}$$

$$L_\mathrm{qd} = \tfrac{\partial\psi_\mathrm{q}(i_\mathrm{d},i_\mathrm{q})}{\partial i_\mathrm{d}} = \tfrac{\partial L_\mathrm{q}(i_\mathrm{d},i_\mathrm{q})}{\partial i_\mathrm{d}}i_\mathrm{q} \approx 0\,, \tag{4d}$$

which eventually yield the dq-current dynamics

$$L_\mathrm{d}(i_\mathrm{d}, i_\mathrm{q})\tfrac{\mathrm{d}}{\mathrm{d}t}i_\mathrm{d} = -Ri_\mathrm{d} + \omega L_\mathrm{q}(i_\mathrm{d}, i_\mathrm{q})i_\mathrm{q} + u_\mathrm{d} \tag{5a}$$

$$L_\mathrm{q}(i_\mathrm{d}, i_\mathrm{q})\tfrac{\mathrm{d}}{\mathrm{d}t}i_\mathrm{q} = -Ri_\mathrm{q} - \omega L_\mathrm{d}(i_\mathrm{d}, i_\mathrm{q})i_\mathrm{d} - \omega\psi_\mathrm{p}(i_\mathrm{q}) + u_\mathrm{q}\,. \tag{5b}$$

In addition, the driving torque of the PMSM can be expressed as

$$T_\mathrm{D}(i_\mathrm{d}, i_\mathrm{q}) = \tfrac{3}{2}z_\mathrm{p}\left(\psi_\mathrm{p}(i_\mathrm{q})i_\mathrm{q} + i_\mathrm{d}i_\mathrm{q}(L_\mathrm{d}(i_\mathrm{d}, i_\mathrm{q}) - L_\mathrm{q}(i_\mathrm{d}, i_\mathrm{q}))\right) \tag{6}$$

with the number of pole pairs z_p. Note that (5) and (6) almost correspond to the classical dq-model (Schröder, 2009) with the exception that

Download English Version:

https://daneshyari.com/en/article/10152097

Download Persian Version:

https://daneshyari.com/article/10152097

Daneshyari.com